Altering lipid droplet homeostasis affects *Coxiella burnetii* intracellular growth

Minal Mulye[1], Brianne Zapata[1,2], and Stacey D. Gilk[1*]

[1] Department of Microbiology and Immunology, Indiana University School of Medicine, Indianapolis, Indiana, United States of America.

[2] Department of Biology, California State University, Dominguez Hills, Carson, California, United States of America.

*Corresponding author: 635 Barnhill Rd, MS 420, Indianapolis, IN 46202. Telephone: 317-274-8028. Fax: 317-278-3331. E-mail: sgilk@iupui.edu

Running title: Lipid droplets during *Coxiella burnetii* infection.

ABSTRACT

Coxiella burnetii is an obligate intracellular bacterial pathogen and a causative agent of culture-negative endocarditis. While *C. burnetii* initially infects alveolar macrophages, it has also been found in lipid droplet (LD)-containing foamy macrophages in the cardiac valves of endocarditis patients. In addition, transcriptional studies of *C. burnetii*-infected macrophages reported differential regulation of the LD coat protein-encoding gene perilipin 2 *(plin-2)*. To further investigate the relationship between LDs and *C. burnetii*, we compared LD numbers in mock-infected and *C. burnetii*-infected alveolar macrophages using fluorescence microscopy. Compared to only 10% of mock-infected cells, 50% of *C. burnetii*-infected cells had more than 50 LDs/cell as early as 24 hours post-infection, indicating a significant increase in LDs in infected cells. Increased LDs required the *C. burnetii* Type 4B Secretion System (T4BSS), a major virulence factor that manipulates host cellular processes by secreting bacterial effector proteins into the host cell cytoplasm. To determine the importance of LDs during *C. burnetii* infection, we assessed the effect of manipulating LD homeostasis on *C. burnetii* intracellular growth. Surprisingly, blocking LD formation with the pharmacological inhibitors triascin C or T863, or knocking out acyl-CoA transferase-1 *(acat-1)* in alveolar macrophages, increased *C. burnetii* growth at least 2-fold. Conversely, preventing LD lipolysis by inhibiting adipose triglyceride lipase (ATGL) with atglistatin almost completely blocked bacterial growth, suggesting LD breakdown is essential for *C. burnetii*. Together these data suggest that LDs are detrimental to *C. burnetii* and maintenance of LD homeostasis, possibly via the T4BSS, is critical for bacterial growth.

39 **IMPORTANCE**

40 Host neutral lipid storage organelles known as lipid droplets (LDs) serve as a source of energy,
41 nutrients, or signaling lipids during infection with intracellular bacteria, such as *Mycobacterium*
42 spp., and *Chlamydia* spp. LDs have also been associated with infection of the intracellular
43 bacterial pathogen *Coxiella burnetii*, a significant cause of culture-negative infectious
44 endocarditis. Although *C. burnetii* was found in LD-rich foam macrophages in endocarditis
45 patients, little is known about the host LD-*C. burnetii* relationship. We demonstrated a *C.*
46 *burnetii* Type 4B Secretion System (T4BSS)-dependent LD accumulation in macrophages,
47 suggesting that the T4BSS plays a key role in regulating host cell LD formation or breakdown.
48 Further, manipulation of LD homeostasis significantly affected *C. burnetii* intracellular growth,
49 indicating LDs play an important role during *C. burnetii* infection. Since *C. burnetii* endocarditis
50 has a 19% mortality rate even in treated patients, exploring the LD-*C. burnetii* association might
51 identify novel therapeutic targets.

52

53 **INTRODUCTION**

54 Lipid droplets (LDs) are dynamic cytoplasmic organelles which store cellular lipids in
55 eukaryotic cells. LDs are uniquely comprised of a phospholipid monolayer surrounding a
56 hydrophobic core of neutral lipids, primarily sterol esters and triacylglycerols. LD assembly
57 begins with neutral lipid synthesis, where fatty acyl CoA synthetases generate long chain fatty
58 acids which are used by acyl-CoA:cholesterol acyltransferase (ACAT) and acyl-
59 CoA:diacylglycerol acyltransferase (DGAT) for formation of sterol esters and triacyglycerols,
60 respectively. After progressive accumulation of neutral lipids in the ER, LD formation occurs
61 primarily by budding of the lipid ester globule surrounded by the cytoplasmic leaflet of the ER

62 membrane (1, 2). LD breakdown and release of free cholesterol and fatty acids is mediated by
63 hormone sensitive lipase (HSL) (3) and adipose triglyceride lipase (ATGL) (4). Functionally,
64 LDs serve as intracellular lipid reservoirs for membrane synthesis or energy metabolism. In
65 addition, LDs are linked to a range of cellular functions including protein storage, protein
66 degradation and signaling (2).

67 LDs are emerging as important players during host-pathogen interactions. During
68 infection of host cells, Hepatitis C virus (HCV) (5) and Dengue virus (6) co-opt LDs as
69 platforms for viral assembly and replication. Even though pharmacological manipulation of LD
70 content reduced viral numbers, the importance of LDs during viral infection still remains elusive
71 (7). Increased LD numbers in host cells is observed upon infection with several pathogens
72 including HCV (5) and Dengue virus (6), as well as the protozoan parasites *Trypanosoma cruzi*
73 (8), *Plasmodium berghei* (9), *Toxoplasma gondii* (10), *Leishmania amazonensis* (11) and
74 *Leishmania major* (12). In addition, the intracellular bacterial pathogens *Chlamydia* spp. (13),
75 *Mycobacterium* spp. (14-17), *Orientia tsutugamushi* (18), and *Salmonella typhimurium* (19) have
76 been reported to increase LD numbers in infected cells. It has been suggested that triacylglycerol
77 and cholesterol esters stored in LDs are a major source of energy and nutrients for *C.*
78 *trachomatis* (13, 20) and *M. tuberculosis* (14). Furthermore, in cells infected with *M. leprae* (21),
79 *M. bovis* (15), *T. cruzi* (22), and *Leishmania infantum chagasi* (23), LDs serve as a source of the
80 eicosanoids such as prostaglandins and leukotrienes, important signaling lipids which modulate
81 inflammation and the immune response. These LD-derived eicosanoids are hypothesized to favor
82 intracellular pathogen survival by downregulating the immune response (24).

83 LDs have been implicated during infection by *Coxiella burnetii*, a gram-negative
84 intracellular bacterium and the causative agent of human Q fever. Primarily spread through

85 aerosols, *C. burnetii* acute infection is characterized by a debilitating flu-like illness, while
86 chronic disease results in endocarditis. Although *in vitro* and *in vivo C. burnetii* can infect a wide
87 range of cells including epithelial cells and fibroblasts, the bacterium first infects alveolar
88 macrophages during natural infection. Inside the host cell, *C. burnetii* directs formation of a
89 specialized lysosome-like compartment called the parasitophorous vacuole (PV) which is
90 essential for *C. burnetii* survival. During establishment of the PV, the *C. burnetii* type 4B
91 secretion system (T4BSS) secretes effector proteins into the host cell cytoplasm, where these
92 bacterial proteins manipulate a wide range of cellular processes. While not established to be
93 T4BSS-dependent, *C. burnetii* is thought to manipulate host cell lipid metabolism, including LDs
94 (25-28). *C. burnetii*-containing LD-filled foam cells were found in heart valves of an infected
95 patient (29), and LDs were observed in the *C. burnetii* PV lumen of infected human alveolar
96 macrophages (30). Further, two separate microarray analyses reported differential regulation of
97 the LD coat protein *plin-2* in *C. burnetii*-infected human macrophage-like cells (THP-1) (27, 28),
98 suggesting *C. burnetii* induced changes in host cell LDs. Intriguingly, siRNA depletion of the
99 phospholipase involved in LD breakdown, PNPLA2 (also known as ATGL), increased the
100 number of *C. burnetii* PVs in HeLa epithelial cells (31). In addition, treatment of monkey kidney
101 epithelial cells (Vero cells) with a broad spectrum antiviral molecule ST699, which localizes to
102 the host cell LDs, inhibited *C. burnetii* intracellular growth (32). Despite these observations, the
103 importance of LDs during *C. burnetii* infection is not known. In this study, we further examined
104 the relationship between host LDs and *C. burnetii*. We observed a T4BSS-dependent increase in
105 LD numbers in infected alveolar and monocyte-derived macrophages. Furthermore,
106 manipulation of LD homeostasis significantly altered *C. burnetii* intracellular growth, thus
107 strongly indicating that LDs play an important role during *C. burnetii* infection.

108

109 **RESULTS AND DISCUSSION**

110 ***C. burnetii* infection results in host cell LD accumulation.**

111 To examine the role of LDs in *C. burnetii* pathogenesis, we first quantitated LDs in infected
112 cells. Previously, two separate microarray studies reported differential regulation of the LD coat
113 protein-encoding gene *plin-2* in *C. burnetii*-infected cells (27, 28), which generally indicates
114 changes in LD numbers. As *C. burnetii* preferentially infects alveolar macrophages during
115 natural infection, we utilized a mouse alveolar macrophage cell line (MH-S) previously shown to
116 be a model for *C. burnetii* infection (33). Cells were stained for the LD coat protein PLIN2 and
117 the LD number per cell was determined using fluorescence microscopy. During a 4-day mock-
118 infection, irrespective of the time point, the majority (~80%) of cells had less than 50 LDs per
119 cell (Figure 1). In contrast, a significant increase in LDs per cell was observed at 1, 2 and 4 days
120 after *C. burnetii* infection, with 50% of infected cells having more than 50 LDs. Notably, LD
121 accumulation was observed as early as 1 day post-infection, when the PV has not expanded and
122 the bacteria are not in log growth. This result suggests that LD accumulation is not a host
123 response to a large PV, but could be due to direct manipulation of host LDs by *C. burnetii*.

124

125 **Host cell LD accumulation is dependent on the *C. burnetii* Type 4B Secretion System**
126 **(T4BSS).**

127 Previously, based on microarray analysis of *C. burnetii*-infected cells where bacterial
128 protein synthesis was blocked, Mahapatra *et al.* identified 36 host cell genes specifically
129 regulated by *C. burnetii* during early stages of infection. These genes were predominantly
130 identified as being involved in innate immune response, cell death and proliferation, vesicular

131 trafficking, cytoskeletal organization and lipid homeostasis. Interestingly, *plin-2* expression level
132 was dependent on *C. burnetii* protein synthesis (27). Together with our data, this suggests that *C.*
133 *burnetii* actively manipulates host LDs as early as day 1 post-infection, possibly through
134 bacterial effector proteins secreted into the host cytoplasm by the *C. burnetii* T4BSS. The *C.*
135 *burnetii* T4BSS detectably secrets effector proteins starting 1 hour post-infection in bone
136 marrow-derived macrophages and 8 hours post-infection in HeLa cells (34). To test if the *C.*
137 *burnetii* T4BSS was responsible for LD accumulation, macrophages were infected with a T4BSS
138 *dotA* mutant and LD numbers analyzed at 1, 2, and 4 days post infection. While at least 75% of
139 the wild-type *C. burnetii*-infected cells had >50 LDs at all timepoints, only 40% cells infected
140 with T4BSS mutant had >50 LDs per cell, similar to mock-infected cells (Figure 2A and B). This
141 suggests the T4BSS is involved in increased LDs in *C. burnetii*-infected alveolar macrophages.

142 To confirm this finding, we analyzed LD numbers in human macrophage-like cells (THP-
143 1). Similar to mouse alveolar macrophages, when compared to mock- or T4SS mutant-infected
144 cells, wild-type *C. burnetii*-infected THP-1 cells had increased LD numbers at 1 and 4 days post-
145 infection (Figure 2C). Interestingly, T4BSS-dependent LD accumulation was not observed at 2
146 days post-infection. However, these results demonstrate that the *C. burnetii*-induced increase in
147 LDs in both human and mouse macrophages is independent of cell type and dependent on the *C.*
148 *burnetii* T4BSS.

149 The requirement for the *C. burnetii* T4BSS suggests that one or more *C. burnetii* T4BSS
150 effector proteins may actively manipulate LDs. Other bacteria have been shown to manipulate
151 host LDs via effector proteins. For example, the *C. trachomatis* LD-associated protein Lda3
152 plays a role in LD translocation into the *Chlamydia*-containing vacuole through localization to
153 the LD surface (20). In addition, the *Salmonella* Typhimurium type 3 secretion system (T3SS)

154 effector protein SseJ esterifies cholesterol and increases LD numbers when expressed in
155 epithelial and macrophage cells (19). While our data demonstrate that the *C. burnetii* T4BSS is
156 involved in LD accumulation, the bacterial effector proteins and the specific LD processes
157 involved remain unknown.
158
159 **Blocking LD formation increases *C. burnetii* growth.**
160 Given our finding that *C. burnetii* appears to actively manipulate host LD accumulation
161 through the T4BSS, we next assessed the importance of LDs during *C. burnetii* infection. We
162 first blocked LD formation using triascin C, a long chain fatty acyl CoA synthetase inhibitor,
163 which blocks overall LD formation (35). Compared to vehicle control, treatment with triascin C
164 significantly reduced LD numbers, with <5 LDs per cell (Figure 3A). We next blocked LD
165 formation and quantitated bacterial growth using a fluorescent infectious focus-forming unit
166 (FFU) assay. At various times post-infection, bacteria were recovered from MH-S cells, replated
167 onto a monolayer of Vero cells, and incubated for 5 days. After staining for *C. burnetii*, the
168 number of fluorescent foci were counted, with 1 focus equivalent to 1 viable bacterium.
169 Compared to vehicle-treated cells, triascin C treatment resulted in a 5-fold increase in *C. burnetii*
170 growth at 4 days post-infection (Figure 3B).
171 To further validate these results, we used CRISPR/Cas-9 to knockout *acat-1* (Figure 3C),
172 the enzyme responsible for sterol esterification. While *acat-1*$^{-/-}$ LDs lack sterol esters, the number
173 of LDs in wild-type and *acat-1*$^{-/-}$ cells appeared to be the same by fluorescence microscopy
174 (Figure 3D). Compared to wild-type cells, *C. burnetii* growth in *acat-1*$^{-/-}$ cells increased by 2 fold
175 at 4 days post-infection (Figure 3E), indicating that blocking sterol esterification is beneficial for
176 *C. burnetii* growth. To further deplete both triacylglycerol-and sterol ester-containing LDs, we

177 treated *acat-1*$^{-/-}$ cells with the DGAT1 inhibitor T863, which specifically blocks formation of
178 triacylglycerols (36). This treatment resulted in significantly fewer LDs than in wild-type or
179 *acat-1*$^{-/-}$ cells (Figure 3D). *C. burnetii* growth increased 2-fold in T863-treated *acat-1*$^{-/-}$ cells
180 compared to vehicle-treated *acat-1*$^{-/-}$ cells (Figure 3F), suggesting that both sterol ester- and
181 triacylglycerol-containing LDs play a significant role during *C. burnetii* growth.

182 These studies demonstrate through both pharmaceutical and genetic approaches that
183 blocking LD formation increases *C. burnetii* fitness in macrophages. Interestingly, Mahapatra *et*
184 *al*. observed an increase in *plin-2* transcript levels after transiently blocking *C. burnetii* protein
185 synthesis, suggesting that wild-type *C. burnetii* downregulates LD formation (27). This raises
186 intriguing questions as to how and why LDs increase in *C. burnetii*-infected macrophages. LD
187 accumulation occurs during inflammatory response in macrophages in atherosclerotic lesions
188 (37), leukocytes from joints of patients with inflammatory arthritis (38), and eosinophils in
189 allergic inflammation (39). Thus, an innate immune response to the T4BSS apparatus or T4BSS
190 effector proteins may increase LDs in *C. burnetii*-infected macrophages. It is also possible that
191 fission of preexisting LDs, and not *de novo* formation, is responsible for increased numbers of
192 LDs (40). As observed in Figure 2A, the LD size in *C. burnetii*-infected macrophages appeared
193 smaller than the mock- or T4BSS mutant-infected macrophages. These smaller LDs might be the
194 result of *C. burnetii* T4BSS-mediated fission of the pre-existing LDs, resulting in increased LD
195 numbers in wild-type bacteria-infected cells.

196

197 **Inhibiting LD breakdown blocks *C. burnetii* growth.**

198 Because blocking LD formation appeared to benefit *C. burnetii,* we next examined *C.*
199 *burnetii* growth after inhibiting LD breakdown and increasing LD numbers. When fatty acids or

200 cholesterol are needed by cells or tissues, triacylglycerols and sterol esters stored in LDs are
201 hydrolyzed by cytosolic lipases such as hormone sensitive lipase (HSL) (2, 3) and adipose
202 triglyceride lipase (ATGL) (4). In our studies, we pharmacologically inhibited ATGL with the
203 selective and competitive inhibitor atglistatin, which binds the ATGL patatin-like phospholipase
204 domain (41). We first measured viability of axenic *C. burnetii* cultures in the presence or
205 absence of atglistatin (Figure 4A). Treatment for 4 days had no effect on axenic *C. burnetii*
206 viability, indicating atglistatin does not directly affect *C. burnetii*.

207 We next tested the effect of atglistatin on intracellular bacteria. After atglistatin treatment
208 of wild-type MH-S cells, we observed larger LDs, although the number did not significantly
209 increase (Figure 3A). Interestingly, *C. burnetii* intracellular growth in atglistatin-treated wild-
210 type MH-S cells was reduced by 5-fold, with essentially no growth (Figure 4B). Further,
211 blocking LD breakdown with atglistatin in *acat-1*$^{-/-}$ cells, which contain predominantly
212 triacylglycerol-containing LDs, also reduced bacterial growth (Figure 4C). Together, these data
213 demonstrate that blocking LD breakdown significantly inhibits intracellular *C. burnetii* growth.

214 Our data suggest that LD breakdown is essential for *C. burnetii* intracellular survival in
215 macrophages. Previously, siRNA knockdown of ATGL in HeLa cells increased the number of *C.*
216 *burnetii* PVs (31). However, *C. burnetii* growth in ATGL-deficient cells was not determined,
217 leaving it unclear how ATGL affect *C. burnetii* growth in epithelial cells Fatty acids liberated
218 during LD breakdown can be reesterified or serve as signaling cofactors, building blocks for
219 membranes, or substrates for β-oxidation to generate energy (2). LD-derived fatty acids may
220 serve as a major source of energy and carbon for several intracellular bacteria. *M. tuberculosis*,
221 which can make its own LDs, converts host-derived fatty acids into triacylglycerol, which is then
222 deposited in bacterial LDs (14). The *M. tuberculosis* lipase has been proposed to release stored

223 bacterial fatty acids, but can also degrade host LD-derived triacylglycerol (42). In *C.*
224 *trachomatis*-infected cells, host LDs may provide triacylglycerol and cholesterol esters for
225 bacterial growth (13). In contrast to *C. trachomatis,* we found that blocking LD formation with
226 traiscin C increased *C. burnetii* growth. While it is unknown if *C. burnetii* uses host fatty acids, it
227 is possible that the unesterified free fatty acids in triascin C-treated cells support *C. burnetii*
228 growth.

229 In addition to serving as a source of free fatty acids, LDs are rich in arachidonic acids and
230 enzymes that generate arachidonic acid-derived inflammatory lipid mediators, such as
231 prostaglandins and leukotrienes (43, 44). In *M. leprae*-infected Schwann cells and *M. bovis*
232 BCG-infected macrophages, increased LD biogenesis correlates with increased production of
233 prostaglandin E2 (PGE2), linking LDs to the production of innate immunity modulators (16, 45).
234 Thus, LDs serve as a source of inflammatory mediators in response to pathogen infection.
235 Interestingly, elevated levels of PGE2 have been observed in *C. burnetii* endocarditis patients
236 and have been linked to *C. burnetii*-mediated immunosuppression. Koster *et al.* reported
237 lymphocytes from chronic Q fever patients were unresponsive to *C. burnetii* antigens, an effect
238 reversed by PGE2 suppression with indomethacin (46). In addition, after stimulation with *C.*
239 *burnetii* antigens, monocytes from Q fever patients produced PGE2, which in turn
240 downregulated IL-2 and IFNγ production by T lymphocytes. This downregulation of pro-
241 inflammatory cytokine production was reversed by PGE2 synthesis inhibitor Piroxicam (47).
242 Thus, while PGE2 appears to play a role in Q fever patients, the relationship between *C.*
243 *burnetii*-induced LDs and PGE2 production is not known. Considering that LD breakdown can
244 serve multiple functions, *C. burnetii* could use LDs either as a source of nutrients or for
245 production of lipid immune mediators like PGE2, which could then modulate the host cell

246 response to promote *C. burnetii* intracellular growth.

247 In summary, our data demonstrate that LD homoeostasis is important for *C. burnetii*
248 intracellular survival. Because the *C. burnetii* T4BSS is involved in LD accumulation,
249 characterizing bacterial T4BSS effector proteins that target host LD homeostasis will help further
250 understand the role of LDs in *C. burnetii* pathogenesis.

251

252 **MATERIALS AND METHODS**

253 Bacteria and mammalian cells

254 *C. burnetii* Nine Mile Phase II (NMII; clone 4, RSA439) were purified from Vero cells (African
255 green monkey kidney epithelial cells, ATCC CCL-81; American Type Culture Collection,
256 Manassas, VA) and stored as previously described (48). For experiments examining T4BSS-
257 dependent accumulation of LDs, NMII and the *dotA* mutant (49) were grown for 4 days in
258 ACCM-2, washed twice with phosphate buffered saline (PBS) and stored as previously described
259 (50). Vero, mouse alveolar macrophages (MH-S; ATCC CRL-2019) and human monocytes
260 (THP-1; ATCC TIB-202) were maintained in RPMI (Roswell Park Memorial Institute) 1640
261 medium (Corning, New York, NY, USA) containing 10% fetal bovine serum (Atlanta
262 Biologicals, Norcross, GA, USA) at 37°C and 5% CO_2 and human embryonic kidney 293
263 (HEK293T; ATCC CRL-3216) in DMEM (Dulbecco's Modified Eagle Medium) (Corning, New
264 York, NY, USA) containing 10% fetal bovine serum at 37°C and 5% CO_2. THP-1 cells were
265 differentiated with 200 nM of phorbol 12-myristate 13-acetate (PMA) for 24 hours. PMA was
266 removed, and the cells rested for 48 hours prior to infection. The multiplicity of infection (MOI)
267 was optimized for each bacterial stock, cell type and infection condition for a final infection of
268 ~1 internalized bacterium/cell at 37°C and 5% CO_2.

269

270 Generating *acat-1*$^{-/-}$ MH-S cell line

271 The guide RNA sequence 5′TCGCGTCTCCATGGCTGCCC3′ to mouse *acat-1* was selected
272 using the optimized CRISPR design site crispr.mit.edu. Oligonucleotides were synthesized (IDT,
273 Coralville, IA, USA), annealed, and cloned into the lentiCRISPRv2 plasmid (a gift from Feng
274 Zhang, Addgene # 52961, Cambridge, MA, USA) (51), at the BsmBI restriction site to generate
275 plentiCRISPRv2-*acat-1*. To generate lentivirus, HEK293T cells were co-transfected with
276 plentiCRISPRv2-*acat-1* and packaging plasmids pVSVg (Addgene # 8454), pRSV-Rev
277 (Addgene # 12253), and pMDLg/pRRE (Addgene # 12251) using FuGENE6 reagent (Promega,
278 Madison, WI, USA). At 48 hours post-transfection, supernatant was collected and centrifuged at
279 3000xg, and then filtered with 0.45µm filter to remove cells and debris. Supernatant was
280 concentrated using the Lenti-X concentrator (Catalog # PT4421-2, Clontech, USA) and viral
281 RNA isolated using Viral RNA isolation kit (Catalog # 740956, Macherey-Nagel, Germany) to
282 determine viral titer using Lenti-X qRT-PCR titration kit (Catalog # PT4006-2, Clontech). Viral
283 titers were optimized for transduction of MH-S cells to generate stable *acat-1*$^{-/-}$ cells.

284 $2x10^5$ MH-S cells were plated in a 6 well plate and transduced with 5.8 x 10^6 viral
285 particles/ml. 1 µg/ml puromycin was used for selection 48 hours post-transduction and continued
286 for 24 hours. The puromycin was then removed and the cells allowed to recover before isolating
287 individual clones by limiting dilution.

288 To confirm disruption of *acat-1*, clones were lysed in 2% SDS (Sigma-Aldrich, St. Louis,
289 MO, USA) for SDS-PAGE and immunoblotting with 1:1000 rabbit anti-mouse ACAT1-specific
290 antibody (Catalog # NBP189285, Novus Biologicals, Littleton, CO, USA) and 1:4000 GAPDH
291 loading control monoclonal antibody (Catalog # MA5-15738, ThermoFisher Scientific,

292 Waltham, MA, USA). The multiplicity of infection (MOI) was optimized for each bacterial stock
293 for a final infection of ~1 internalized bacterium/cell.
294
295 LD quantitation
296 $1x10^5$ MH-S cells were plated onto ibidi-treated channel μslide $VI^{0.4}$ ($3x10^3$ cells per channel;
297 Ibidi, Verona, WI) and allowed to adhere overnight. After infecting with *C. burnetii* for 1 hour,
298 cells were gently washed with phosphate buffered saline (PBS) to remove extracellular bacteria,
299 and incubated in 10% FBS-RPMI. At different times post-infection, infected cells were fixed
300 with 2.5% paraformaldehyde on ice for 15 min, then permeabilized/blocked for 15 min with
301 0.1% saponin and 1% bovine serum albumin (BSA) in PBS (saponin-BSA-PBS) and stained
302 with 1:1000 rabbit anti-mouse PLIN2 primary antibody (Catalog # PA1-16972, ThermoFisher
303 Scientific), 1:2000 guinea-pig anti-*C. burnetii* primary antibody (52) and 1:1000 rat anti-LAMP
304 (Catalog # 553792, BD Biosciences) primary antibody in saponin-BSA-PBS for 1 hour. THP-1
305 cells were stained with 1:500 guinea-pig anti-human PLIN2 primary antibody (Catalog # 20R-
306 AP002, Fitzgerald Industries International, Acton, MA), 1:2000 rabbit anti-*C. burnetii* primary
307 antibody and 1:1000 rat anti-LAMP primary antibody in saponin-BSA-PBS for 1 hour. After
308 three washes with PBS, cells were stained with 1:2000 AlexaFluor 488 anti-rabbit, AlexaFluor
309 594 anti-guinea pig and AlexaFluor 647 anti-rat secondary antibodies (Invitrogen) for 1 hour.
310 ProLong Gold mount (Invitrogen) was added to the wells after washing with PBS and slides
311 visualized on a Leica inverted DMI6000B microscope (100X oil). The number of LDs per cell
312 was quantitated for 50 cells per condition in three individual experiments, with only bacteria-
313 containing cells counted for *C. burnetii*-infected cells. Each experiment was done in duplicate.
314

315 Inhibitors

316 Each LD homeostasis inhibitor used was diluted in DMSO based on manufacturer's instructions
317 and optimum inhibitor concentration was determined based on 100% host cell viability
318 determined by trypan blue staining, and changes in LD numbers per cell. The optimum
319 concentrations determined for each inhibitor was: Triascin C (Enzo Life Sciences, Farmingdale,
320 NY, USA) – 10 μM, T863 (Sigma-Aldrich) – 10 μM, Atglistatin (Cayman Chemicals, Ann
321 Arbor, MI, USA) – 20 μM.

322

323 *C. burnetii* growth by fluorescent infectious focus-forming unit (FFU) assay.

324 To measure growth of *C. burnetii* in wild-type and *acat-1*$^{-/-}$ MH-S cells, $5x10^4$ cells/well were
325 infected for 1 hour in a 48 well plate, washed with PBS, and then incubated with media
326 containing respective vehicle and inhibitors. At the indicated time points, the media was
327 removed and cells were incubated with sterile water for 5 min, pipetted up and down and the
328 lysate diluted 1:5 in 2% FBS-RPMI. Serial dilutions were added to 24 well plate containing
329 confluent monolayers of Vero cells, incubated for 5 days, fixed with methanol and stained with
330 rabbit anti-*C. burnetii* antibody as well as DAPI to confirm monolayer integrity. Four fields per
331 well were captured on an Evos automated microscope (ThermoFisher) with 4X objective and
332 fluorescent foci units were quantitated using ImageJ. Each experiment was done in duplicate.

333

334 Atglistatin-treatment of *C. burnetii* axenic cultures

335 To test bacterial sensitivity to atglistatin, ACCM-2 was inoculated at approximately $1x10^5$
336 bacteria/ml with *C. burnetii* NMII and grown for 3 days as previously described (50). Bacteria
337 (500 μl) were then incubated with DMSO or atglistatin in 24 well plates under normal *C.*

338 *burnetii* culture conditions. Media was replenished every 24 hours by centrifuging the
339 supernatant at 20000xg for 10 min, and bacterial pellet resuspended in new media containing
340 inhibitor. After 4 days, bacteria were diluted 1:10 in 2% FBS-RPMI and serial dilutions were
341 added to confluent Vero cell monolayers in a 96 well ibidi-treated µplate. At 5 days post-
342 infection, the plate was stained and fluorescent foci were determined as above. Each experiment
343 was done in duplicate.
344
345 Statistical analysis
346 Statistical analyses were performed using ordinary one-way ANOVA or two-way ANOVA with
347 Tukey's or Bonferroni's multiple comparisons test in Prism (GraphPad Software, Inc., La Jolla,
348 CA).
349
350 **FIGURE LEGENDS:**
351 **Figure 1: *C. burnetii* infection leads to host cell LD accumulation.**
352 MH-S macrophages were infected with *C. burnetii* NMII and at different times post-infection,
353 cells were stained for PLIN2 (LDs), LAMP1 (PV marker) and *C. burnetii*. LDs were observed by
354 fluorescence microscopy and number of LDs per cell was quantitated. The percent of counted
355 cells containing 0-20, 21-50 and >50 LDs per cell at respective times were plotted. Error bars
356 show the mean of 3 independent experiments +/- SEM * =p<0.05, ** =p <0.01, *** =p <0.001
357 compared to respective >50 LDs/cell in mock-infected cells as determined by two-way ANOVA
358 with Tukey post-hoc test.
359

360 **Figure 2: Host cell LD accumulation is dependent on the *C. burnetii* T4BSS Secretion**
361 **System (T4BSS).**
362 A) Representative images of mock, wild-type *C. burnetii* NMII and T4BSS *(dotA)* mutant-
363 infected MH-S macrophages stained for PLIN2 (LDs) at day 1 post-infection imaged at 100X.
364 Scale bar = 10 µm
365 B) MH-S macrophages and (C) THP-1 monocyte-derived macrophages were infected with wild-
366 type *C. burnetii* NMII and *dotA* mutant. At different time points post-infection, cells were
367 stained for PLIN2 (LDs), LAMP1 (PV marker) and *C. burnetii*. The number of LDs per cell
368 were counted by fluorescence microscopy. Percent of cells containing 0-20, 21-50 and >50 LDs
369 per cell at respective time points were plotted. Error bars show the mean of 3 independent
370 experiments +/- SEM * =p<0.05 compared to respective >50 LDs/cell in *dotA* mutant-infected
371 cells as determined by two-way ANOVA with Tukey post-hoc test.
372
373 **Figure 3: Blocking LD formation increases *C. burnetii* growth.**
374 *C. burnetii* NMII growth in infected MH-S cells treated with different inhibitors was measured at
375 2 and 4 days post-infection by FFU assay.
376 A) Representative images for wild-type MH-S macrophages treated with inhibitors, fixed,
377 stained for PLIN2 (LDs) and imaged day 1 post-treatment at 100X. Scale bar = 10 µm
378 B) Growth in LD formation inhibitor triascin C–treated (10 µM) wild-type MH-S macrophages.
379 Error bars represent the mean of 4 independent experiments +/- SEM. **= p <0.01 compared to
380 vehicle treated cells as determined by two-way ANOVA with Bonferroni post-hoc test.
381 C) ACAT1 protein expression in wild-type and *acat-1*$^{-/-}$ macrophages. Cell lysates were
382 immunoblotted and ACAT1 protein levels were compared with GAPDH as loading control.

383 D) Representative images for vehicle-treated wild-type MH-S macrophages and vehicle and
384 T863-treated *acat-1*$^{-/-}$ macrophages fixed, stained for PLIN2 (LDs) and imaged day 1 post-
385 treatment at 100X. Scale bar = 10 μm
386 E) *C. burnetii* NMII growth in vehicle-treated wild-type and *acat-1*$^{-/-}$ MH-S macrophages and (F)
387 T863-treated wild-type and *acat-1*$^{-/-}$ MH-S macrophages. Error bars represent the mean of 3
388 independent experiments +/- SEM., * =p<0.05, *** =p <0.001 as determined by two-way
389 ANOVA with Bonferroni post-hoc test.
390
391 **Figure 4: Inhibiting LD breakdown blocks *C. burnetii* growth.**
392 Effect of ATGL inhibitor atglistatin on viability of axenic and intracellular *C. burnetii* was
393 determined by FFU assay.
394 A) Direct effect of atglistatin on *C. burnetii* NMII. Atglistatin was added to axenic *C. burnetii*
395 NMII cultures and bacterial viability was determined at day 4 using FFU assay. Error bars
396 represent the mean of 3 independent experiments +/- SEM. ns = not significant compared to
397 vehicle treatment as determined by ordinary one-way ANOVA with Tukey post-hoc test.
398 B) Growth in atglistatin-treated (20 μM) and vehicle-treated wild-type MH-S macrophages.
399 Error bars represent the mean of 4 independent experiments +/- SEM. *= p <0.05, ****
400 =p<0.0001 compared to vehicle-treated cells as determined by two-way ANOVA with
401 Bonferroni post-hoc test.
402 C) Growth in atglistatin-treated (20 μM) and vehicle-treated *acat-1*$^{-/-}$ MH-S macrophages. Error
403 bars represent the mean of 4 independent experiments +/- SEM. ** =p<0.01 compared to vehicle
404 treated cells as determined by two-way ANOVA with Bonferroni post-hoc test.
405

406 **ACKNOWLEDGMENTS**

407 This research was supported by National Institutes of Health (AI21786; S.D.G.), American Heart
408 Association (16POST27250157; M.M.) and National Institutes of Health (5R25GM07592; B.Z.).
409 We thank Anna Justis, Tatiana Clemente and Rajshekar Gaji for critical reading of the
410 manuscript and members of the IU Biology of Intracellular Pathogens Group for helpful
411 suggestions.

412 We have no conflicts of interest to declare.

413

414 **REFERENCES**

415

416 1. **Pol A, Gross SP, Parton RG.** 2014. Review: biogenesis of the multifunctional lipid
417 droplet: lipids, proteins, and sites. The Journal of Cell Biology **204:**635-646.
418 2. **Walther TC, Farese RV, Jr.** 2012. Lipid droplets and cellular lipid metabolism. Annual
419 Review of Biochemistry **81:**687-714.
420 3. **Vaughan M, Berger JE, Steinberg D.** 1964. Hormone-Sensitive Lipase and
421 Monoglyceride Lipase Activities in Adipose Tissue. The Journal of Biological Chemistry
422 **239:**401-409.
423 4. **Haemmerle G, Lass A, Zimmermann R, Gorkiewicz G, Meyer C, Rozman J,**
424 **Heldmaier G, Maier R, Theussl C, Eder S, Kratky D, Wagner EF, Klingenspor M,**
425 **Hoefler G, Zechner R.** 2006. Defective lipolysis and altered energy metabolism in mice
426 lacking adipose triglyceride lipase. Science **312:**734-737.
427 5. **Filipe A, McLauchlan J.** 2015. Hepatitis C virus and lipid droplets: finding a niche.
428 Trends in Molecular Medicine **21:**34-42.
429 6. **Samsa MM, Mondotte JA, Iglesias NG, Assuncao-Miranda I, Barbosa-Lima G, Da**
430 **Poian AT, Bozza PT, Gamarnik AV.** 2009. Dengue virus capsid protein usurps lipid
431 droplets for viral particle formation. PLoS Pathogens **5:**e1000632.
432 7. **Herker E, Ott M.** 2012. Emerging role of lipid droplets in host/pathogen interactions.
433 Journal of Biological Chemistry **287:**2280-2287.
434 8. **D'Avila H, Freire-de-Lima CG, Roque NR, Teixeira L, Barja-Fidalgo C, Silva AR,**
435 **Melo RC, Dosreis GA, Castro-Faria-Neto HC, Bozza PT.** 2011. Host cell lipid bodies
436 triggered by *Trypanosoma cruzi* infection and enhanced by the uptake of apoptotic cells
437 are associated with prostaglandin E(2) generation and increased parasite growth. Journal
438 of Infectious Disease **204:**951-961.
439 9. **Pulido-Mendez M, Finol HJ, Giron ME, Aguilar I.** 2006. Ultrastructural pathological
440 changes in mice kidney caused by *Plasmodium berghei* infection. Journal of
441 Submicroscopic Cytology and Pathology **38:**143-148.

442 10. **Charron AJ, Sibley LD.** 2002. Host cells: mobilizable lipid resources for the
443 intracellular parasite *Toxoplasma gondii*. Journal of Cell Science **115:**3049-3059.
444 11. **Lecoeur H, Giraud E, Prevost MC, Milon G, Lang T.** 2013. Reprogramming neutral
445 lipid metabolism in mouse dendritic leucocytes hosting live *Leishmania amazonensis*
446 amastigotes. PLoS Neglected Tropical Diseases **7:**e2276.
447 12. **Rabhi S, Rabhi I, Trentin B, Piquemal D, Regnault B, Goyard S, Lang T,**
448 **Descoteaux A, Enninga J, Guizani-Tabbane L.** 2016. Lipid Droplet Formation, Their
449 Localization and Dynamics during *Leishmania major* Macrophage Infection. PLoS One
450 **11:**e0148640.
451 13. **Kumar Y, Cocchiaro J, Valdivia RH.** 2006. The obligate intracellular pathogen
452 *Chlamydia trachomatis* targets host lipid droplets. Current Biology **16:**1646-1651.
453 14. **Daniel J, Maamar H, Deb C, Sirakova TD, Kolattukudy PE.** 2011. *Mycobacterium*
454 *tuberculosis* uses host triacylglycerol to accumulate lipid droplets and acquires a
455 dormancy-like phenotype in lipid-loaded macrophages. PLoS Pathogens **7:**e1002093.
456 15. **D'Avila H, Melo RC, Parreira GG, Werneck-Barroso E, Castro-Faria-Neto HC,**
457 **Bozza PT.** 2006. *Mycobacterium bovis* bacillus Calmette-Guerin induces TLR2-mediated
458 formation of lipid bodies: intracellular domains for eicosanoid synthesis *in vivo*. Journal
459 of Immunology **176:**3087-3097.
460 16. **D'Avila H, Roque NR, Cardoso RM, Castro-Faria-Neto HC, Melo RC, Bozza PT.**
461 2008. Neutrophils recruited to the site of *Mycobacterium bovis* BCG infection undergo
462 apoptosis and modulate lipid body biogenesis and prostaglandin E production by
463 macrophages. Cellular Microbiology **10:**2589-2604.
464 17. **Mattos KA, Lara FA, Oliveira VG, Rodrigues LS, D'Avila H, Melo RC, Manso PP,**
465 **Sarno EN, Bozza PT, Pessolani MC.** 2011. Modulation of lipid droplets by
466 *Mycobacterium leprae* in Schwann cells: a putative mechanism for host lipid acquisition
467 and bacterial survival in phagosomes. Cellular Microbiology **13:**259-273.
468 18. **Ogawa M, Fukasawa M, Satoh M, Hanada K, Saijo M, Uchiyama T, Ando S.** 2014.
469 The intracellular pathogen *Orientia tsutsugamushi* responsible for scrub typhus induces
470 lipid droplet formation in mouse fibroblasts. Microbes and Infection **16:**962-966.
471 19. **Nawabi P, Catron DM, Haldar K.** 2008. Esterification of cholesterol by a type III
472 secretion effector during intracellular Salmonella infection. Molecular Microbiology
473 **68:**173-185.
474 20. **Cocchiaro JL, Kumar Y, Fischer ER, Hackstadt T, Valdivia RH.** 2008. Cytoplasmic
475 lipid droplets are translocated into the lumen of the *Chlamydia trachomatis*
476 parasitophorous vacuole. PNAS **105:**9379-9384.
477 21. **Mattos KA, D'Avila H, Rodrigues LS, Oliveira VG, Sarno EN, Atella GC, Pereira**
478 **GM, Bozza PT, Pessolani MC.** 2010. Lipid droplet formation in leprosy: Toll-like
479 receptor-regulated organelles involved in eicosanoid formation and *Mycobacterium*
480 *leprae* pathogenesis. Journal of Leukocyte Biology **87:**371-384.
481 22. **Toledo DA, Roque NR, Teixeira L, Milan-Garces EA, Carneiro AB, Almeida MR,**
482 **Andrade GF, Martins JS, Pinho RR, Freire-de-Lima CG, Bozza PT, D'Avila H,**
483 **Melo RC.** 2016. Lipid Body Organelles within the Parasite *Trypanosoma cruzi*: A Role
484 for Intracellular Arachidonic Acid Metabolism. PLoS One **11:**e0160433.
485 23. **Araujo-Santos T, Rodriguez NE, Moura-Pontes S, Dixt UG, Abanades DR, Bozza**
486 **PT, Wilson ME, Borges VM.** 2014. Role of prostaglandin F2alpha production in lipid

487 bodies from *Leishmania infantum chagasi*: insights on virulence. Journal of Infectious
488 Disease **210:**1951-1961.
489 24. **Melo RC, Weller PF.** 2016. Lipid droplets in leukocytes: Organelles linked to
490 inflammatory responses. Experimental Cell Research **340:**193-197.
491 25. **Justis AV, Hansen B, Beare PA, King KB, Heinzen RA, Gilk SD.** 2016. Interactions
492 between the *Coxiella burnetii* parasitophorous vacuole and the endoplasmic reticulum
493 involve the host protein ORP1L. Cellular Microbiology doi:10.1111/cmi.12637.
494 26. **Martinez E, Allombert J, Cantet F, Lakhani A, Yandrapalli N, Neyret A, Norville**
495 **IH, Favard C, Muriaux D, Bonazzi M.** 2016. *Coxiella burnetii* effector CvpB
496 modulates phosphoinositide metabolism for optimal vacuole development. PNAS
497 **113:**E3260-3269.
498 27. **Mahapatra S, Ayoubi P, Shaw EI.** 2010. *Coxiella burnetii* Nine Mile II proteins
499 modulate gene expression of monocytic host cells during infection. BMC Microbiology
500 **10:**244.
501 28. **Ren Q, Robertson SJ, Howe D, Barrows LF, Heinzen RA.** 2003. Comparative DNA
502 microarray analysis of host cell transcriptional responses to infection by *Coxiella burnetii*
503 or *Chlamydia trachomatis*. Annals of the New York Academy of Sciences **990:**701-713.
504 29. **Brouqui P, Dumler JS, Raoult D.** 1994. Immunohistologic demonstration of *Coxiella*
505 *burnetii* in the valves of patients with Q fever endocarditis. The American Journal of
506 Medicine **97:**451-458.
507 30. **Graham JG, MacDonald LJ, Hussain SK, Sharma UM, Kurten RC, Voth DE.** 2013.
508 Virulent *Coxiella burnetii* pathotypes productively infect primary human alveolar
509 macrophages. Cellular Microbiology **15:**1012-1025.
510 31. **McDonough JA, Newton HJ, Klum S, Swiss R, Agaisse H, Roy CR.** 2013. Host
511 pathways important for *Coxiella burnetii* infection revealed by genome-wide RNA
512 interference screening. MBio **4:**e00606-00612.
513 32. **Sandoz KM, Valiant WG, Eriksen SG, Hruby DE, Allen RD, 3rd, Rockey DD.** 2014.
514 The broad-spectrum antiviral compound ST-669 restricts chlamydial inclusion
515 development and bacterial growth and localizes to host cell lipid droplets within treated
516 cells. Antimicrobial Agents and Chemotherapy **58:**3860-3866.
517 33. **Soltysiak KA, van Schaik EJ, Samuel JE.** 2015. Surfactant protein D binds to *Coxiella*
518 *burnetii* and results in a decrease in interactions with murine alveolar macrophages. PLoS
519 One **10:**e0136699.
520 34. **Newton HJ, McDonough JA, Roy CR.** 2013. Effector protein translocation by the
521 *Coxiella burnetii* Dot/Icm type IV secretion system requires endocytic maturation of the
522 pathogen-occupied vacuole. PLoS One **8:**e54566.
523 35. **Igal RA, Wang P, Coleman RA.** 1997. Triacsin C blocks *de novo* synthesis of
524 glycerolipids and cholesterol esters but not recycling of fatty acid into phospholipid:
525 evidence for functionally separate pools of acyl-CoA. The Biochemical Journal **324 (Pt**
526 **2):**529-534.
527 36. **Cao J, Zhou Y, Peng H, Huang X, Stahler S, Suri V, Qadri A, Gareski T, Jones J,**
528 **Hahm S, Perreault M, McKew J, Shi M, Xu X, Tobin JF, Gimeno RE.** 2011.
529 Targeting Acyl-CoA:diacylglycerol acyltransferase 1 (DGAT1) with small molecule
530 inhibitors for the treatment of metabolic diseases. The Journal of Biological Chemistry
531 **286:**41838-41851.

532 37. **Paul A, Chang BH, Li L, Yechoor VK, Chan L.** 2008. Deficiency of adipose
533 differentiation-related protein impairs foam cell formation and protects against
534 atherosclerosis. Circulation Research **102:**1492-1501.
535 38. **Bozza PT, Payne JL, Morham SG, Langenbach R, Smithies O, Weller PF.** 1996.
536 Leukocyte lipid body formation and eicosanoid generation: cyclooxygenase-independent
537 inhibition by aspirin. PNAS **93:**11091-11096.
538 39. **Vieira-de-Abreu A, Calheiros AS, Mesquita-Santos FP, Magalhaes ES, Mourao-Sa**
539 **D, Castro-Faria-Neto HC, Bozza MT, Bandeira-Melo C, Bozza PT.** 2011. Cross-talk
540 between macrophage migration inhibitory factor and eotaxin in allergic eosinophil
541 activation forms leukotriene C(4)-synthesizing lipid bodies. American Journal of
542 Respiratory Cell and Molecular Biology **44:**509-516.
543 40. **Long AP, Manneschmidt AK, VerBrugge B, Dortch MR, Minkin SC, Prater KE,**
544 **Biggerstaff JP, Dunlap JR, Dalhaimer P.** 2012. Lipid droplet *de novo* formation and
545 fission are linked to the cell cycle in fission yeast. Traffic **13:**705-714.
546 41. **Mayer N, Schweiger M, Romauch M, Grabner GF, Eichmann TO, Fuchs E, Ivkovic**
547 **J, Heier C, Mrak I, Lass A, Hofler G, Fledelius C, Zechner R, Zimmermann R,**
548 **Breinbauer R.** 2013. Development of small-molecule inhibitors targeting adipose
549 triglyceride lipase. Nature Chemical Biology **9:**785-787.
550 42. **Deb C, Daniel J, Sirakova TD, Abomoelak B, Dubey VS, Kolattukudy PE.** 2006. A
551 novel lipase belonging to the hormone-sensitive lipase family induced under starvation to
552 utilize stored triacylglycerol in *Mycobacterium tuberculosis*. The Journal of Biological
553 Chemistry **281:**3866-3875.
554 43. **Dvorak AM, Dvorak HF, Peters SP, Shulman ES, MacGlashan DW, Jr., Pyne K,**
555 **Harvey VS, Galli SJ, Lichtenstein LM.** 1983. Lipid bodies: cytoplasmic organelles
556 important to arachidonate metabolism in macrophages and mast cells. Journal of
557 Immunology **131:**2965-2976.
558 44. **Weller PF, Monahan-Earley RA, Dvorak HF, Dvorak AM.** 1991. Cytoplasmic lipid
559 bodies of human eosinophils. Subcellular isolation and analysis of arachidonate
560 incorporation. The American Journal of Pathology **138:**141-148.
561 45. **Mattos KA, Oliveira VG, D'Avila H, Rodrigues LS, Pinheiro RO, Sarno EN,**
562 **Pessolani MC, Bozza PT.** 2011. TLR6-driven lipid droplets in *Mycobacterium leprae*-
563 infected Schwann cells: immunoinflammatory platforms associated with bacterial
564 persistence. Journal of Immunology **187:**2548-2558.
565 46. **Koster FT, Williams JC, Goodwin JS.** 1985. Cellular immunity in Q fever: modulation
566 of responsiveness by a suppressor T cell-monocyte circuit. Journal of Immunology
567 **135:**1067-1072.
568 47. **Izzo AA, Marmion BP.** 1993. Variation in interferon-gamma responses to *Coxiella*
569 *burnetii* antigens with lymphocytes from vaccinated or naturally infected subjects.
570 Clinical and Experimental Immunology **94:**507-515.
571 48. **Cockrell DC, Beare PA, Fischer ER, Howe D, Heinzen RA.** 2008. A method for
572 purifying obligate intracellular *Coxiella burnetii* that employs digitonin lysis of host cells.
573 Journal of Microbiological Methods **72:**321-325.
574 49. **Beare PA, Gilk SD, Larson CL, Hill J, Stead CM, Omsland A, Cockrell DC, Howe**
575 **D, Voth DE, Heinzen RA.** 2011. Dot/Icm type IVB secretion system requirements for
576 *Coxiella burnetii* growth in human macrophages. MBio **2:**e00175-00111.

50. **Omsland A, Cockrell DC, Howe D, Fischer ER, Virtaneva K, Sturdevant DE, Porcella SF, Heinzen RA.** 2009. Host cell-free growth of the Q fever bacterium *Coxiella burnetii*. PNAS **106:**4430-4434.
51. **Sanjana NE, Shalem O, Zhang F.** 2014. Improved vectors and genome-wide libraries for CRISPR screening. Nature Methods **11:**783-784.
52. **Coleman SA, Fischer ER, Howe D, Mead DJ, Heinzen RA.** 2004. Temporal analysis of *Coxiella burnetii* morphological differentiation. The Journal of Bacteriology **186:**7344-7352.

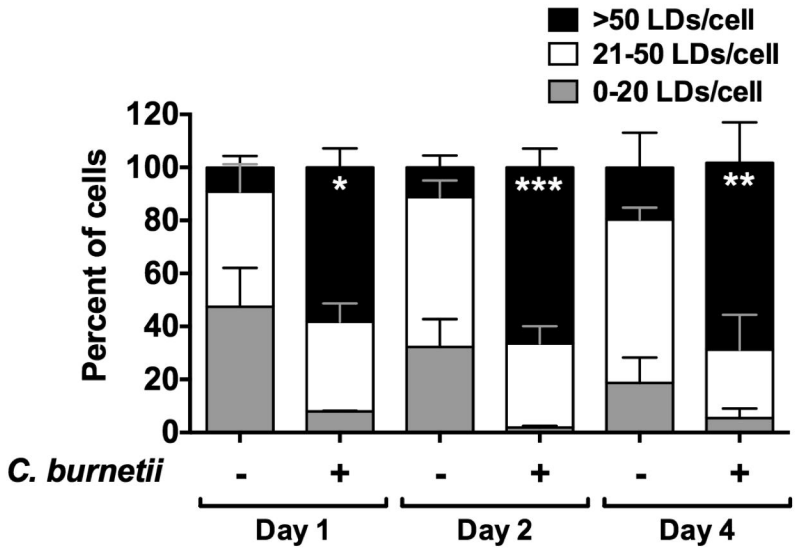

Figure 1: *C. burnetii* infection leads to host cell LD accumulation.
MH-S macrophages were infected with *C. burnetii* NMII and at different times post-infection, cells were stained for PLIN2 (LDs), LAMP1 (PV marker) and *C. burnetii*. LDs were observed by fluorescence microscopy and number of LDs per cell was quantitated. The percent of counted cells containing 0-20, 21-50 and >50 LDs per cell at respective times were plotted. Error bars show the mean of 3 independent experiments +/- SEM * =p<0.05, ** =p <0.01, *** =p <0.001 compared to respective >50 LDs/cell in mock-infected cells as determined by two-way ANOVA with Tukey post-hoc test.

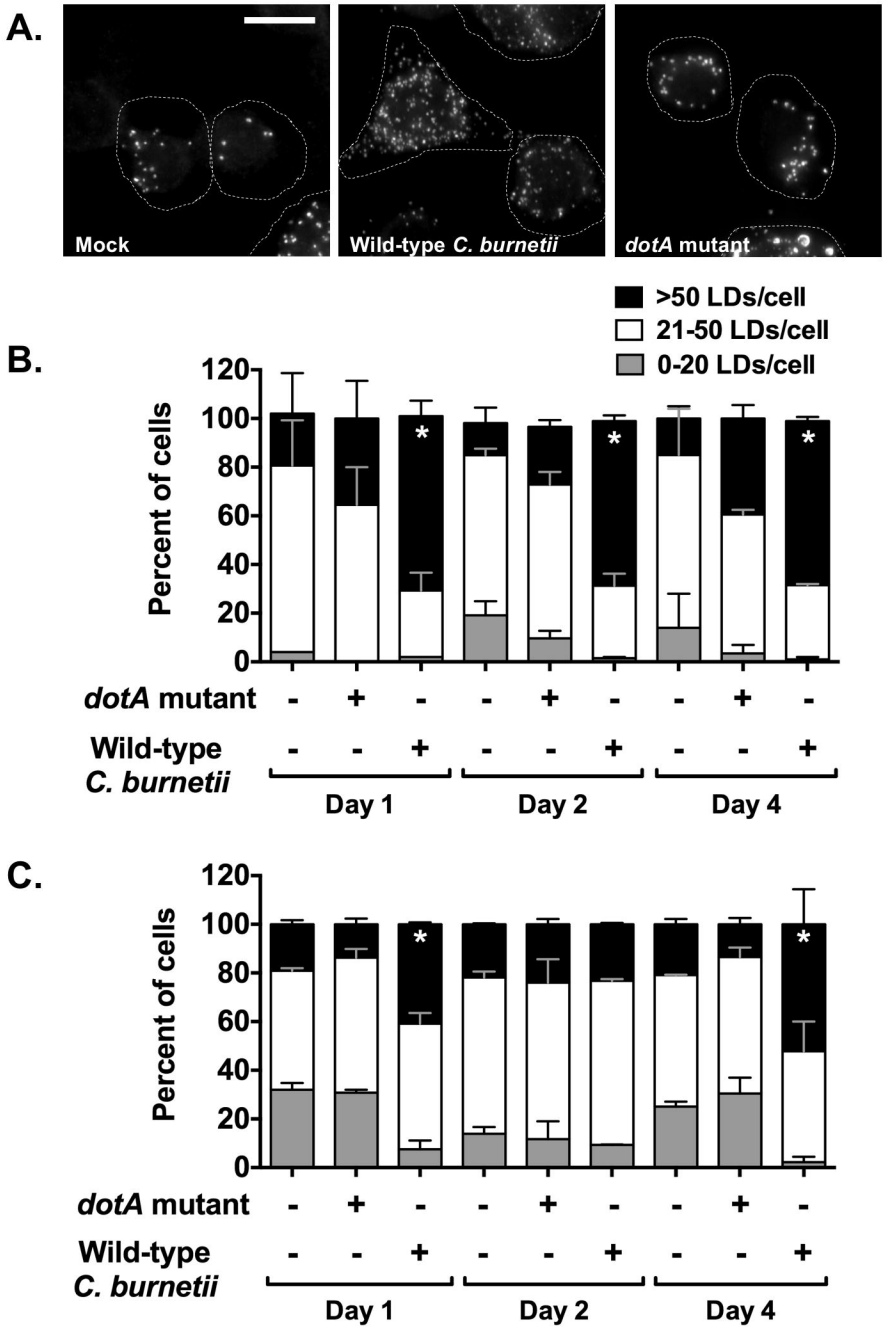

Figure 2: Host cell LD accumulation is dependent on the *C. burnetii* T4BSS Secretion System (T4BSS).

A) Representative images of mock, wild-type *C. burnetii* NMII and T4BSS *(dotA)* mutant-infected MH-S macrophages stained for PLIN2 (LDs) at day 1 post-infection imaged at 100X. Scale bar = 10 µm

B) MH-S macrophages and (C) THP-1 monocyte-derived macrophages were infected with wild-type *C. burnetii* NMII and *dotA* mutant. At different time points post-infection, cells were stained for PLIN2 (LDs), LAMP1 (PV marker) and *C. burnetii*. The number of LDs per cell were counted by fluorescence microscopy. Percent of cells containing 0-20, 21-50 and >50 LDs per cell at respective time points were plotted. Error bars show the mean of 3 independent experiments +/- SEM * =$p<0.05$ compared to respective >50 LDs/cell in *dotA* mutant-infected cells as determined by two-way ANOVA with Tukey post-hoc test.

Figure 3: Blocking LD formation increases *C. burnetii* growth.

C. burnetii NMII growth in infected MH-S cells treated with different inhibitors was measured at 2 and 4 days post-infection by FFU assay.

A) Representative images for wild-type MH-S macrophages treated with inhibitors, fixed, stained for PLIN2 (LDs) and imaged day 1 post-treatment at 100X. Scale bar = 10 µm

B) Growth in LD formation inhibitor triascin C–treated (10 µM) wild-type MH-S macrophages. Error bars represent the mean of 4 independent experiments +/- SEM. **= $p < 0.01$ compared to vehicle treated cells as determined by two-way ANOVA with Bonferroni post-hoc test.

C) ACAT1 protein expression in wild-type and *acat-1*$^{-/-}$ macrophages. Cell lysates were immunoblotted and ACAT1 protein levels were compared with GAPDH as loading control.

D) Representative images for vehicle-treated wild-type MH-S macrophages and vehicle and T863-treated *acat-1*$^{-/-}$ macrophages fixed, stained for PLIN2 (LDs) and imaged day 1 post-treatment at 100X. Scale bar = 10 µm

E) *C. burnetii* NMII growth in vehicle-treated wild-type and *acat-1*$^{-/-}$ MH-S macrophages and (F) T863-treated wild-type and *acat-1*$^{-/-}$ MH-S macrophages. Error bars represent the mean of 3 independent experiments +/- SEM., * =$p<0.05$, *** =$p < 0.001$ as determined by two-way ANOVA with Bonferroni post-hoc test.

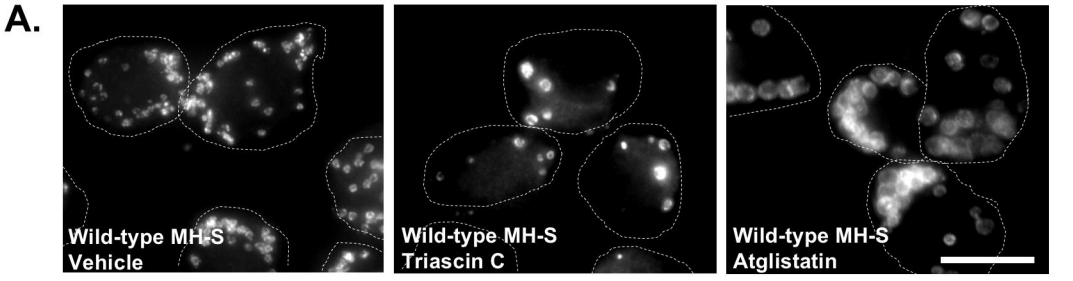

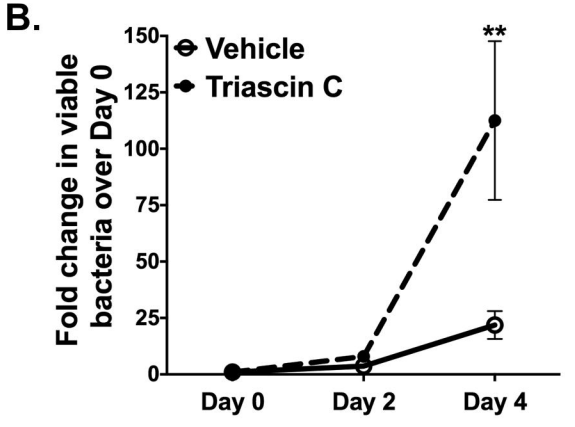

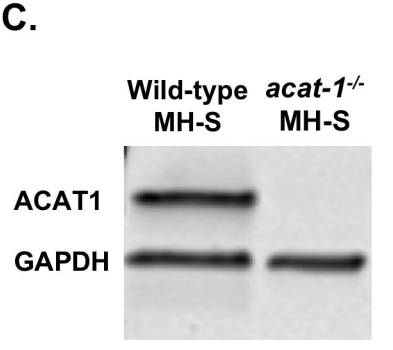

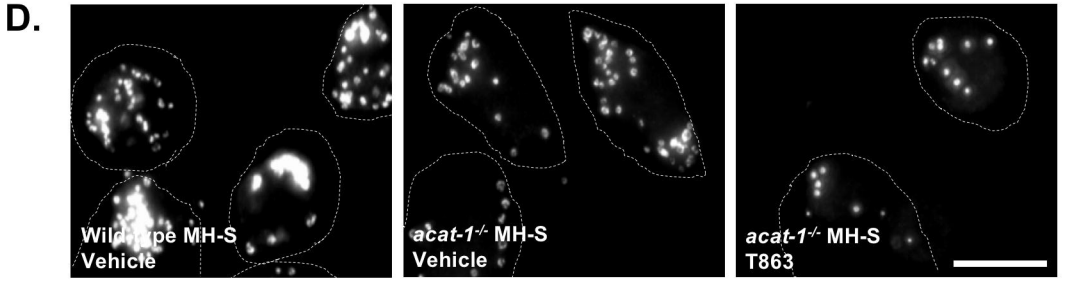

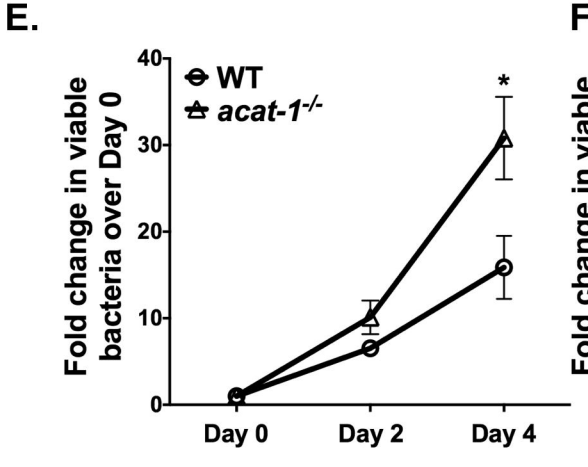

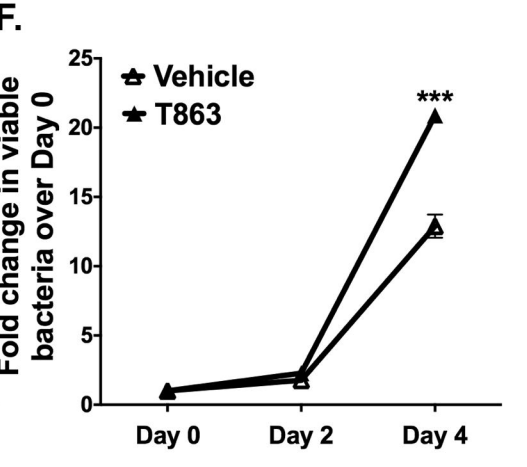

Figure 3: Blocking LD formation increases *C. burnetii* growth.

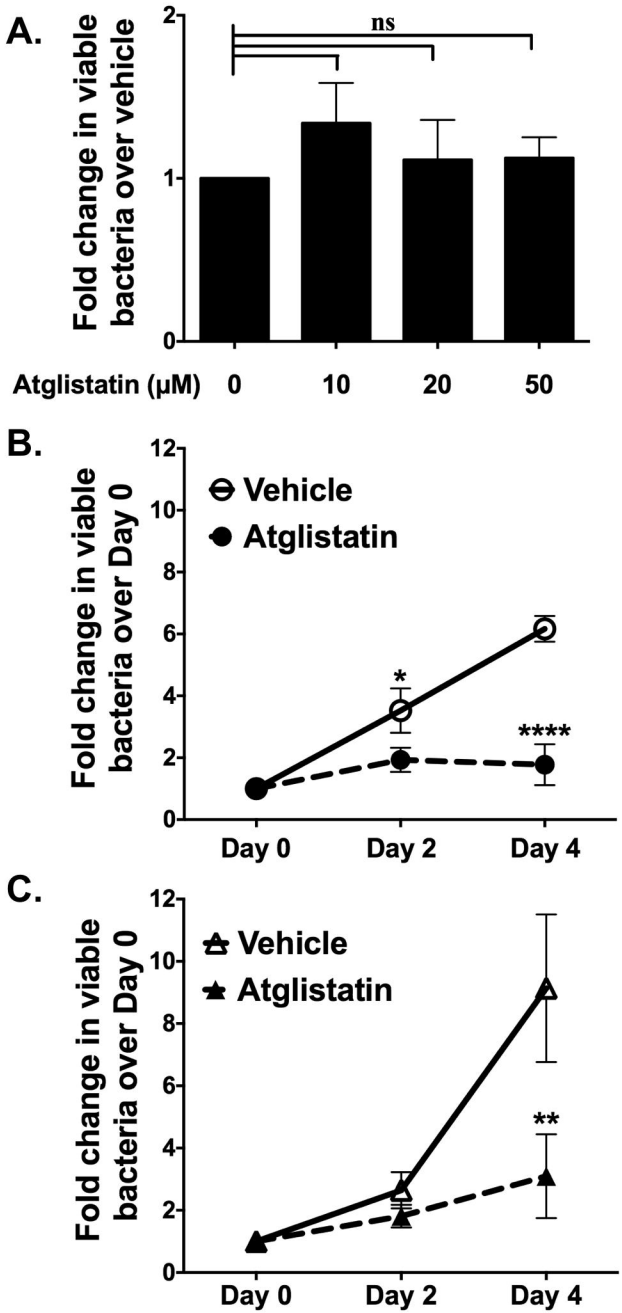

Figure 4: Inhibiting LD breakdown blocks *C. burnetii* growth.

Effect of ATGL inhibitor atglistatin on viability of axenic and intracellular *C. burnetii* NMII was determined by FFU assay.

A) Direct effect of atglistatin on *C. burnetii* NMII. Atglistatin was added to axenic *C. burnetii* cultures and bacterial viability was determined at day 4 using FFU assay. Error bars represent the mean of 3 independent experiments +/- SEM. ns = not significant compared to vehicle treatment as determined by ordinary one-way ANOVA with Tukey post-hoc test.

B) Growth in atglistatin-treated (20 μM) and vehicle-treated wild-type MH-S macrophages. Error bars represent the mean of 4 independent experiments +/- SEM. *= $p < 0.05$, **** $=p<0.0001$ compared to vehicle-treated cells as determined by two-way ANOVA with Bonferroni post-hoc test.

C) Growth in atglistatin-treated (20 μM) and vehicle-treated *acat-1*$^{-/-}$ MH-S macrophages. Error bars represent the mean of 4 independent experiments +/- SEM. ** $=p<0.01$ compared to vehicle treated cells as determined by two-way ANOVA with Bonferroni post-hoc test.